Available online at www.sciencedirect.com

ScienceDirect

Procedia CIRP 82 (2019) 497–502

www.elsevier.com/locate/procedia

17th CIRP Conference on Modelling of Machining Operations

Model-based Planning of Machining Operations for Industrial Robots

F. Schnoes[a,*], M. F. Zaeh[a]

[a]*iwb – Institute for Machine Tools and Industrial Management, Technical University of Munich, Boltzmannstrasse 15, 85748 Garching, Germany*

Abstract

The static and dynamic mechanical properties of standard industrial robots differ strongly from common CNC-machines. For robot-based machining operations, these properties have to be considered. In this paper, a method for the optimal placement of the workpiece within the workspace, the design of the machining process and the compensation of toolpath deviations during the machining process of metallic workpieces is presented. The method is based on a coupled machine-process-model and the derivation of performance, accuracy and reliability indicators. The method was validated by the machining of aluminum workpieces and the evaluation of the accuracy improvement due to the multi-axis compensation mechanism.

Peer-review under responsibility of the scientific committee of The 17th CIRP Conference on Modelling of Machining Operations

Keywords: Robot Machining; Simulation; Process Force; Process Planning; Volumetric Modeling; Machining Strategy

1. Introduction

In comparison to conventional CNC machine tools, industrial robots are very flexible, have a small footprint, require low investment costs and have a large workspace. These benefits are mainly achieved by the serial kinematic structure of the robots. However, industrial robots are also less accurate and not as stiff as conventional machine tools [1]. These negative properties significantly depend on the pose of the robot and lead to a decreased accuracy of the workpiece, low frequency oscillations and chatter marks on the workpiece surface [2]. For robot-based machining applications of hard materials (e.g. aluminum or steel) the process forces significantly influence the achievable workpiece accuracy. The dominant influences on the path accuracy of machining robots are listed in Figure 1.

2. State of the Art

Two main approaches are used to improve the machining performance and accuracy of milling robots. Offline-strategies are used to generate compensated part programs while online-strategies are used to enhance the workpiece accuracy in a control loop with force or position feedback. Roesch introduces a model based online approach for the compensation of static path deflections for milling robots based on an analytic stiffness model of the robot and a stationary force measurement sensor [4]. Reinl et al. show a model-based approach for the offline simulation and compensation of static path deviations during the machining process [5]. Berger and Soernmo show a combined online-offline-approach for the compensation of static deflections during the machining process by combining a position tracking system with a piezo-actuated micro manipulator [6], [7]. Gotlih et al. present a method to determine the pose dependent accuracy of the robotic milling system based on a division of the dextrous workspace into regions with sufficient and insufficient accuracy [8]. Besides the accuracy improvement of the workpiece and the compensation of static offsets, the stability of the robotic machining process has to be considered. Halbauer et al. show that adapted machining strategies with constant transitions between toolpath segments can improve the geometric accuracy and surface quality of the workpiece [9]. Mousavi et al. present a method to predict the machining stability based on a matrix structural analysis model of a robot [10] and the stability criterion of Budak and Altintas [11]. Xiong et al. demonstrate the optimization of the feed-direction based on a directional stiffness index [12]. While the presented methods show a significant improvement of the accuracy and stability due to single influences, a holistic method for the planning of robot-based machining processes is still missing. In this paper we pro-

* Corresponding author. Tel.: +49-089-289-15441 ; fax: +49-089-289-15111.

E-mail address: florian.schnoes@iwb.mw.tum.de (F. Schnoes).

2212-8271
Peer-review under responsibility of the scientific committee of The 17th CIRP Conference on Modelling of Machining Operations
10.1016/j.procir.2019.04.331

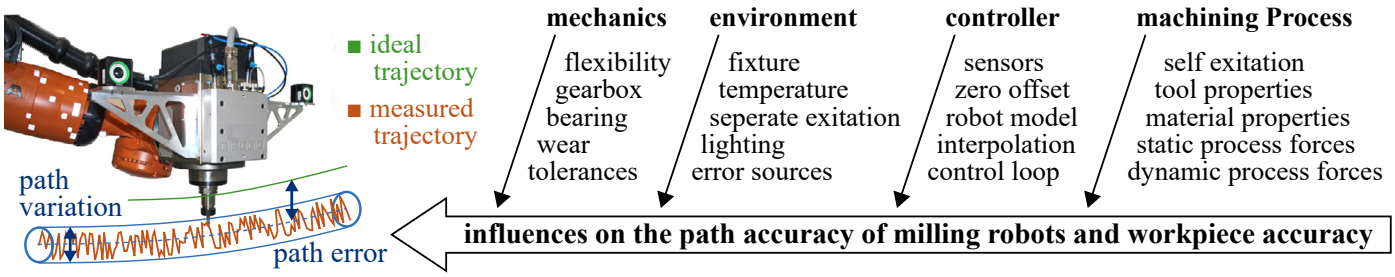

Fig. 1. Influences on the path accuracy of milling robots. Based on [3, p.1403].

pose a model-based method for the offline planning of robotic machining processes, which ensures a stable machining behavior and increases the accuracy of the machined workpiece. The method focuses on the placement of the workpiece within the workspace, the design of the machining process and the compensation of the remaining deflections. The hardware used for the validation of the method consists of a Kuka KR240 robot and a high-speed milling spindle.

3. Model-based Accuracy Improvement of Milling Robots

In order to increase the performance and accuracy of machining robots, we introduce a sequential model-based approach. The method (see Figure 2) is based on a flexible dynamic model of the robotic milling system and a process force model of the machining process. In the first step of the method, the position and orientation of the workpiece is optimized in dependence on the properties of the robot and the process. In the second step of the method, the design of the machining process is adjusted based on the anisotropic robot stiffness and in order to reduce the self-excitation of the robotic milling system. In the third step of the method, the remaining toolpath deviations are simulated and reduced by offline compensation mechanisms.

4. Model of the Robotic Machining System

The main sources of flexibility of the robot are represented in a lumped flexibility model with compliant joints. Additional virtual compliant joints are defined for the lower and upper arm of the robot to account for the structural bending of the components. The resulting kinematic chain (see Figure 3) is described by a series of coordinate transformations. The parameters for the transformation are given in Table 1. The individual joint transformations are given by equation 1, where θ_i is the rotation around the i-th z-axis, α_i is the rotation around the i-th x-axis and x_i, y_i and z_i are translations along the i-th base vectors (see Equation 1).

$$ {}^{i-1}T_i = \begin{bmatrix} c\theta_i & -s\theta_i & 0 & x_i \\ c\alpha_i \cdot s\theta_i & c\alpha_i \cdot c\theta_i & -s\alpha_i & y_i \cdot c\alpha_i - z_i \cdot s\alpha_i \\ s\alpha_i \cdot s\theta_i & s\alpha_i \cdot c\theta_i & c\alpha_i & y_i \cdot s\alpha_i + z_i \cdot s\alpha_i \\ 0 & 0 & 0 & 1 \end{bmatrix} \quad (1) $$

,with $s\xi \equiv \sin(\xi)$ and $c\xi \equiv \cos(\xi)$.

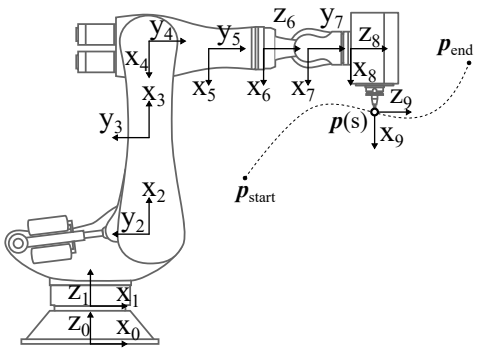

Fig. 3. Graphical representation of the link coordinate systems and of a generic toolpath $\boldsymbol{p}(s)$.

Each coordinate frame represents a bushing joint with infinite translational stiffness and finite rotational stiffness. The rotational stiffness of the bushing joints for the six actuated joints (1, 2, 4, 6, 7, 8) and two virtual joints (3, 5) are given in Table 2 (in accordance with [4]).

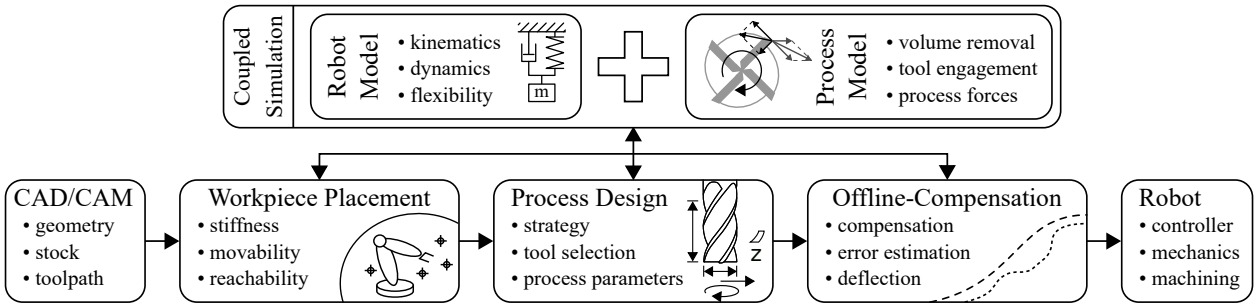

Fig. 2. Sequential method for the improvement of the machining performance of milling robots.

Table 1. Transformation parameters for the defined coordinate systems.

i	θ_i in rad	α_i in rad	x_i in mm	y_i in mm	z_i in mm
1	$-q_1$	0.0	0.0	0.0	225.0
2	$-q_2$	$\pi/2$	350.0	450.0	0.0
3	0.0	0.0	575.0	0.0	0.0
4	$-q_3$	0.0	575.0	0.0	0.0
5	0.0	0.0	41.0	340.0	0.0
6	$-q_4$	$-\pi/2$	0.0	0.0	340.0
7	$-q_5$	$\pi/2$	0.0	320.0	0.0
8	$-q_6$	$-\pi/2$	0.0	0.0	200.0
9	0.0	0.0	tool length	0.0	205.5

Table 2. Torsional joint stiffness of the robotic milling system based on a Kuka KR240 R2500 (see [4]).

stiffness in	joint							
10^7 N / rad	1	2	3	4	5	6	7	8
x	1.603	1.310	0.957	0.736	0.377	0.325	0.253	0.219
axis y	1.603	1.310	0.426	0.736	0.272	0.325	0.253	0.219
z	0.582	0.810	1.136	0.517	1.325	0.106	0.120	0.045

The static deflection $\Delta\boldsymbol{p}$ of the tool center point (TCP) under an external load $\boldsymbol{F}_{ext} = [F_x, F_y, F_z, M_x, M_y, M_z]$ at a given joint configuration $\boldsymbol{q}$ are calculated under the assumption of a negligible complementary stiffness matrix $\boldsymbol{K}_C$ (see [13]):

$$\Delta\boldsymbol{p} \approx \boldsymbol{J}(\boldsymbol{q})\boldsymbol{K}_{\theta}^{-1}\boldsymbol{J}(\boldsymbol{q})^T\boldsymbol{F}_{ext} \tag{2}$$

The kinematic manipulator Jacobian $\boldsymbol{J}(\boldsymbol{q})$ defines the mapping between the generalized degrees of freedom and the Cartesian TCP velocity. The joint stiffness matrix $\boldsymbol{K}_\theta$ is a constant diagonal matrix of the joint stiffnesses of Table 1. The dynamic model of the robot is based on the Articulated Rigid Body Algorithm (see [14]). The necessary spatial inertias of the bodies are computed based on the geometry and total mass of the robot. The algorithm is implemented by utilizing the rigid-body dynamics library (RBDL) [15]. For the dynamic coupling of external loads, the load wrench $\boldsymbol{F}_{ext}$ acting on the TCP is transformed into torques in joint space $\tau_{ext} = \boldsymbol{J}^T\boldsymbol{F}_{ext}$. These torques are included in the forward dynamics solution $\ddot{\boldsymbol{q}} = FD(\boldsymbol{q}, \dot{\boldsymbol{q}}, \boldsymbol{\tau})$, where $\boldsymbol{\tau} = \boldsymbol{\tau}_{act} + \boldsymbol{\tau}_{stiff} + \boldsymbol{\tau}_{ext}$ describes the generalized torques resulting from the actuation, the joint stiffness and the external forces.

5. Process Force Model

For robotic milling systems, large workpiece volumes have to be modeled with a high spatial resolution. The size of the possible workpiece volume can easily exceed 50 m^3. During the milling process, each tooth of the rotating tool removes material from the workpiece and therefore alters the workpiece geometry. Each engagement between a tooth of the tool and the workpiece has to be modeled in order to accurately simulate the process forces. The simulation is separated into a computationally efficient and spatially accurate volume removal simulation (0.001 mm^3 volumetric resolution) and an accurate process force simulation with a high temporal resolution (360 time steps per revolution of the tool). The volume removal simulation is based on a volumetric voxel model of the workpiece and a geometrical model of the tool envelope. Similar to Octree models, the voxel model is based on hierarchical layers with increasing spatial resolution. In order to equalize the memory consumption between in-memory data addresses and volume information, a dynamic subdivision rate of the voxel volumes is implemented. This approach has shown high performance for the representation of sparse volumes in computer graphics [16].

Based on the intersection of the tool and the workpiece, an engagement histogram is computed for each discrete time step of the simulation. The histogram can be interpreted as the unrolled lateral and lower face surface of the tool envelope and shows the intersection as a binary image. The engagement between the single flutes of the tool and the workpiece is computed by projecting the flutes onto the histogram. The angle

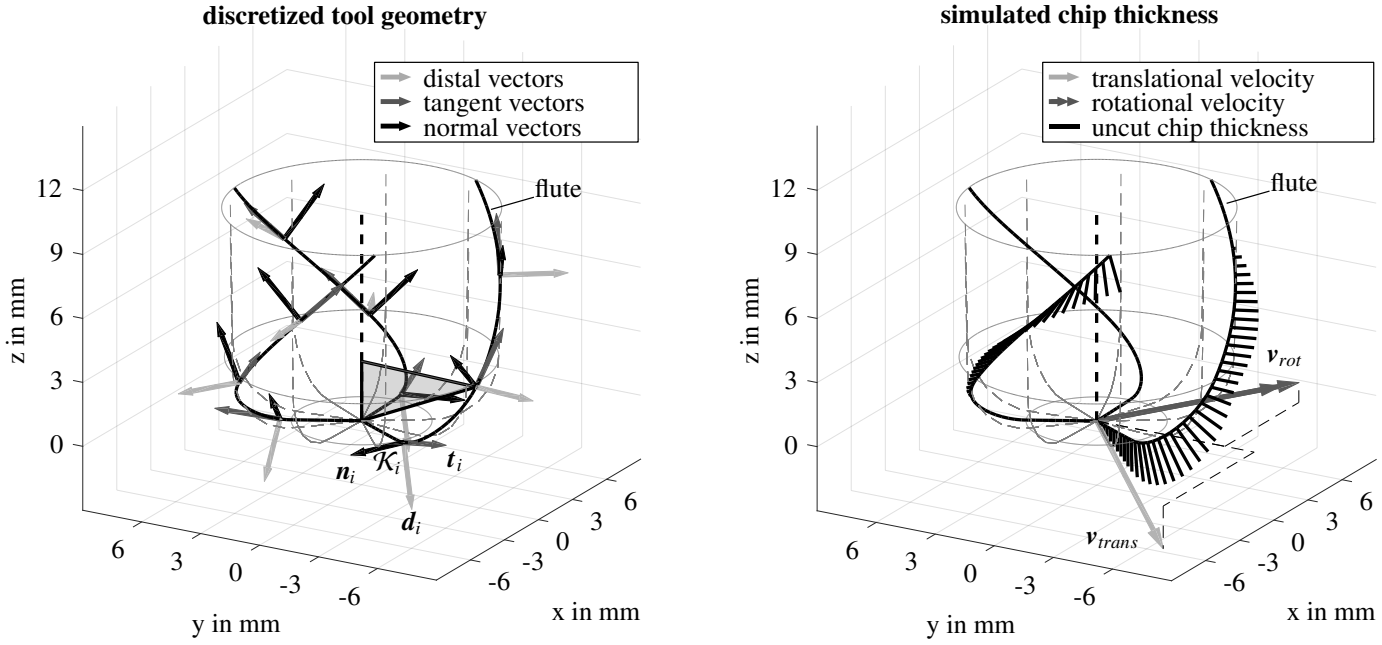

Fig. 4. Visualization of the local tool geometry and the local coordinate systems for finite flute segments (left) and the simulated uncut chip thickness (right).

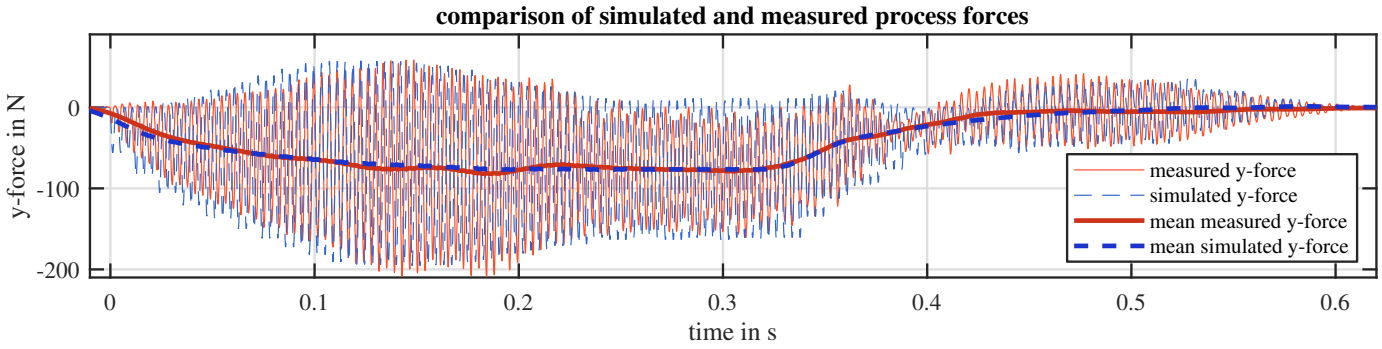

Fig. 5. Comparison of simulated and measured process forces.

offset of each flute is determined by the current tool rotation. By assuming, that the engagement changes are slow compared to the spindle speed and flute rotation, the temporal resolution can be increased without increasing the spatial resolution of the volume removal simulation. For the calculation of the process forces, the flutes are divided into discrete segments with a length of 0.1 mm. The intersecting finite flute segments of the discretized tool are given by the subset $\mathcal{C} \in \mathcal{F}$ of all finite flute segments $\mathcal{F}$. The cutting forces are calculated based on an adapted model of Altintas et al. [17].

In contrast to the model of Altintas et al., each discrete flute segment is represented by a local flute aligned coordinate system. The local coordinate system $\mathcal{K}_i$ is defined by the position of the discrete flute segment $\boldsymbol{r}_i$, a tangential component $\boldsymbol{t}_i$ along the flute, a distal component $\boldsymbol{d}_i$ pointing in outwards direction and a normal component $\boldsymbol{n}_i$ pointing along the direction of the cutting velocity. For discretized flute geometries, the local vectors are computed according to equation 4, 6 and 7. The local uncut chip thickness h_i (see eq. 9) is calculated based on the spindle speed n, the number of flutes z, the translational velocity $\boldsymbol{v}_{trans}$ and the rotational velocity $\boldsymbol{v}_{rot}$. The velocities include the ideal tool movement and the tool movement resulting from oscillations of the dynamic robot model. In contrast to existing models, the uncut chip thickness is calculated numerically based on the flute aligned distal vectors instead of analytically [18]. This approach facilitates the representation of arbitrary flute profiles.

$$\text{flute segment length: } db = |\boldsymbol{r}_{i+1} - \boldsymbol{r}_i| \tag{3}$$

$$\text{tangential component: } \boldsymbol{t_i} = (\boldsymbol{r}_{i+1} - \boldsymbol{r}_i) \,/\, db \tag{4}$$

$$\text{cutting direction: } \boldsymbol{v}_{c,i} = (\boldsymbol{r}_i \times \boldsymbol{z}) \,/\, |\boldsymbol{r}_i \times \boldsymbol{z}| \tag{5}$$

$$\text{distal component: } \boldsymbol{d}_i = (\boldsymbol{t}_i \times \boldsymbol{v}_{c,i}) \,/\, |\boldsymbol{t}_i \times \boldsymbol{v}_{c,i}| \tag{6}$$

$$\text{normal component: } \boldsymbol{n}_i = (\boldsymbol{d}_i \times \boldsymbol{t}_i) \,/\, |\boldsymbol{d}_i \times \boldsymbol{t}_i| \tag{7}$$

$$\text{periodic flute time: } dt = 1 \,/\, (n \cdot z) \tag{8}$$

$$\text{chip thickness: } h_i = \boldsymbol{d}_i \cdot (\boldsymbol{v}_{trans} + \boldsymbol{v}_{rot} \times \boldsymbol{r}_i) \cdot dt \tag{9}$$

The discretized tool geometry and simulated chip thickness are visualized for a 12 mm diameter tool with three flutes and a corner radius of 3 mm. The corresponding uncut chip thicknesses (scaled by a factor of 5) for a translational feed velocity $\boldsymbol{v}_{trans} = [-8 \; -8 \; 2]^T \frac{mm}{s}$ and a rotational feed velocity $\boldsymbol{v}_{rot} = [0.07 \; -0.07 \; 0.01]^T \frac{rad}{s}$ are shown in Figure 4. For each engaged finite flute segment $\mathcal{S}_{i\in\mathcal{C}}$, the finite tangential, distal and normal cutting forces $d\boldsymbol{F}_{t,i}$, $d\boldsymbol{F}_{r,i}$ and $d\boldsymbol{F}_{a,i}$ are calculated and aggregated to the total instantaneous cutting force $\boldsymbol{F}_{ext}$:

$$\boldsymbol{F}_{ext} = \sum_{i\in\mathcal{C}} \begin{bmatrix} \boldsymbol{t}_i & \boldsymbol{d}_i & \boldsymbol{n}_i \end{bmatrix} \begin{bmatrix} k_{te} + k_{tc} \cdot h_i \\ k_{de} + k_{dc} \cdot h_i \\ k_{ne} + k_{nc} \cdot h_i \end{bmatrix} \cdot db \tag{10}$$

For the milling of aluminium EN AW-2007 with an examplary shaft endmill with a 12 mm diameter and a helix angle of 45°, the process force parameters are given in table 3:

Table 3. Examplary process force parameters.

$k_{te} = 4.63\,^{N}/_{mm}$	$k_{tc} = 57.5\,^{N}/_{mm^2}$
$k_{de} = -11.8\,^{N}/_{mm}$	$k_{dc} = -76.5\,^{N}/_{mm^2}$
$k_{ne} = -11.0\,^{N}/_{mm}$	$k_{nc} = -672\,^{N}/_{mm^2}$

Figure 5 shows the measured and simulated process forces of the 12 mm shaft endmill entering and exiting a workpiece. For this experiment, the workpiece material aluminum EN AW-2007, a radial depth of cut $a_e = 12$ mm, an axial depth of cut $a_p = 6$ mm, an uncut chip thickness $fz = 0.08$ mm, a spindle speed $n = 5310$ 1/min and a feed direction in positive y-direction are specified. The dynamic and mean process forces show a good agreement with the measured forces. The root mean squared error of the mean process forces for 80 different cutting conditions is smaller than 10% ≈ 15 N.

6. Workpiece Placement

The workpiece position within the workspace of the robotic milling system influences the coupled machine-process properties. For the optimization of the workpiece position, the toolpath is discretized with a step width of 10 mm resulting in n discrete poses $\boldsymbol{p}_i$ along the toolpath. The optimization objective is the mean deflection $\overline{|\Delta \boldsymbol{p}|} = \frac{1}{n} \sum_{i=1}^{n} \Delta \boldsymbol{p}_i$ of the discretized toolpath with precomputed static process forces. A constrained simulated annealing algorithm with multiple random starting points is used to minimize the objective function. The optimization is constrained by the reachability, the freedom of collision and the available workspace. The available workspace is defined as an axis-aligned bounding box. The translational position and the rotation around the up-vector of the world coordinate system

(equal to $\boldsymbol{Z}_0$ in Figure 3) are used as optimization variables. The optimization improves the achievable workpiece accuracy and avoids an improper positioning of the workpiece within the workspace. The subsequent design of the process is based on the optimized workpiece position and relies on a coupled machine process simulation.

7. Process Design

The goal for the design of the process is the achievement of high material removal rates (MRR) with a high stability reserve (SR). The MRR and the SR are influenced by the tool, the workpiece material, the process parameters and the toolpath. Given a rectangular pocket as target geometry, the tool is selected based on the smallest inner radius. The stiffness of the robot manipulator is anisotropic. Compared to loads in x_0-direction, static forces in y_0-direction induce deflections, which are approximately five times larger. By selecting the radial immersion of the tool in dependence on the feed direction, the mean force direction is adapted to account for the anisotropic stiffness of the robotic system (see Figure 6):

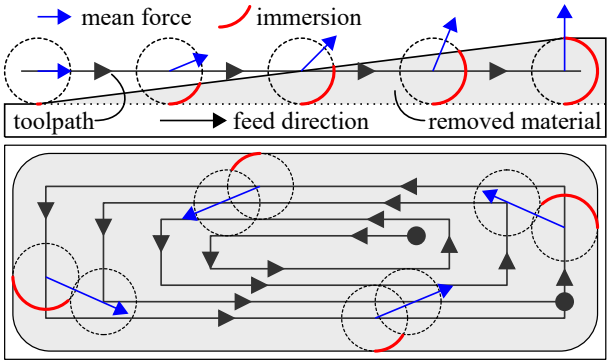

Fig. 6. Control of the mean process force direction by adaption of the radial tool immersion.

The spindle speed n and axial depth of cut a_p are selected based on directional stability lobes for the given cutting conditions (see [2]). The computation of the directional stability lobes is based on measured direct TCP frequency response functions (FRFs) (see [19, pp.258–276]). Based on a feed direction occupancy map, the smallest present maximum depth of cut $b_{cr,\min}$ is selected. The method for the selection of the axial depth is locally valid, but does not account for the nonlinear stiffness properties of the joints and the pose-dependent dynamic system behavior.

8. Offline-Compensation

The selection of a favorable position within the workspace and the machine dependent design of the process improves the machining of the workpiece. However, there is still a remaining deflection of the TCP during the machining operation, which has to be compensated. The coupled machine process model is used to simulate the translational and rotational deflection during the machining operation. The simulated deflection $\Delta\boldsymbol{p}(s)$ at the traveled length s of the toolpath is mirrored and superimposed on the ideal toolpath $\boldsymbol{s}_{ideal}(s)$:

$$\boldsymbol{p}_{comp}(s) = \boldsymbol{p}_{ideal}(s) - \Delta\boldsymbol{p}(s) \tag{11}$$

The compensated toolpath $\boldsymbol{p}_{comp}(s)$ is used for the generation of compensated robot programs. The toolpath is represented by linear movements with a interpolation distance of $\Delta s = 0.3$ mm. Smaller interpolation distances lead to a reduced feedrate due to the limited interpretation speed of current robot controllers. During the actual machining operation, the robot is forced back to the ideal toolpath due to the process forces. For the execution of the generated part programs, no additional sensor or control systems are needed. Therefore, the workspace of the robot is not restricted and no additional real time data processing systems are needed. Although no sensor systems are needed, online methods can be combined with the presented offline compensation. In this case, the offline compensation mechanism is used as a feedforward controller and enables high path accuracies during rapid process force changes.

9. Results and Conclusion

The presented method was implemented in C++ and is able to generate machine code for Kuka robot controllers. For commonly used tool diameters, the simulation is faster than the actual machining process. The input file for the method is a CAM-generated ideal toolpath. For the representation of the toolpath, the APT file format is used. The ideal toolpath includes all informations for the workpiece placement, the process design, the process force simulation and the offline compensation. For the process force simulation, the APT file has to be annotated with the given stock material dimensions. The method was validated by machining a workpiece with variable depth of cut. The workpiece includes two slots, which are machined subsequently. The geometry of the stock material resembles a stairway. The stairway geometry leads to axial depths of cut a_p ranging from 1 mm to 7 mm for each slot. During the machining of each slot, the process forces successively increase and vanish rapidly at the exit of the workpiece. The slot on the left side is machined with deactivated, the slot on the right side with activated compensation mechanism. Figure 7 shows the reduction of the maximum machining error of a workpiece with variable depth of cut by over 90 % (1.2 mm to 0.11 mm).

The presented method provides a promising approach for the utilization of robotic milling systems for the machining of hard materials. By considering the coupled machine process behavior during the workpiece placement, the process design and the compensation of static deflections, the potentials of using industrial robots for machining operations are expanded. The utilization of additional error-prone and cost-intensive sensor systems are avoided by solely relying on models of the robot and the machining process. The method was implemented as a semi-automated post-processor and facilitates the generation of part programs for machining robots.

By introducing a flute geometry considering process model, the range of validity of the process force parameters were ex-

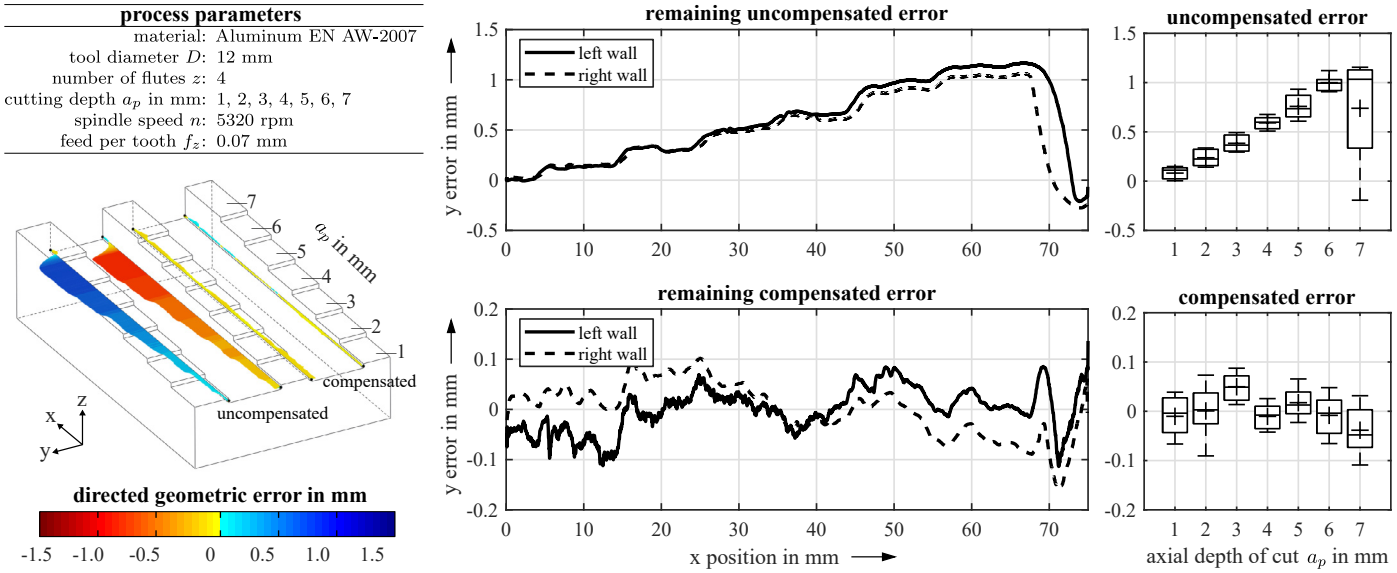

Fig. 7. Error reduction by applying the presented method to a workpiece with variable depth of cut.

tended for changes in the tool geometry. A further extension of the process force model for different workpiece materials could increase the scope of application. The process design is currently based on measured TCP frequency response functions. In the future the method will be extended to include simulated TCP-FRFs. The identification of the dynamic robot model parameters requires intricate measurement procedures. Therefore specialized methods for the identification of the model parameters of machining robots are needed. The process design could be further improved by a dynamic feed rate optimizer. As a result, smoother compensation profiles could be generated by reducing the feed rate at positions with strong changes of the engagement conditions.

10. Acknowledgements

We gratefully acknowledge the support of the Siemens AG and the support by R. Rosen, D. Hartmann, U. Wever, B. Obst, D. Regulin, T. Kamps, S. Tauchmann, D. Bitterolf and F. Fischer.

References

[1] U. Schneider, M. Ansaloni, M. Drust, F. Leali, A. Verl, Experimental investigation of sources of error in robot machining, in: Robotics in Smart Manufacturing, Springer, 2013, pp. 14–26.

[2] M. F. Zaeh, O. Roesch, Improvement of the machining accuracy of milling robots, Production Engineering 8 (6) (2014), pp. 737–744.

[3] B. Siciliano, O. Khatib, Springer handbook of robotics, Springer, 2016.

[4] O. Roesch, Steigerung der Arbeitsgenauigkeit bei der Fräsbearbeitung metallischer Werkstoffe mit Industrierobotern, Vol. 302, Herbert Utz Verlag, 2015.

[5] C. Reinl, M. Friedmann, J. Bauer, M. Pischan, E. Abele, O. Von Stryk, Model-based off-line compensation of path deviation for industrial robots in milling applications, in: Advanced Intelligent Mechatronics (AIM), 2011 IEEE/ASME International Conference on, IEEE, 2011, pp. 367–372.

[6] U. Berger, M. Halbauer, C. Lehmann, D. Euhus, J. P. Städter, Präzisionsfräsen mit industrierobotern, ZWF Zeitschrift für wirtschaftlichen Fabrikbetrieb 107 (7-8) (2012), pp. 533–536.

[7] O. Sörnmo, B. Olofsson, U. Schneider, A. Robertsson, R. Johansson, Increasing the milling accuracy for industrial robots using a piezo-actuated high-dynamic micro manipulator, in: Advanced Intelligent Mechatronics (AIM), 2012 IEEE/ASME International Conference on, IEEE, 2012, pp. 104–110.

[8] J. Gotlih, M. Brezocnik, J. Balic, T. Karner, B. Razborsek, K. Gotlih, Determination of accuracy contour and optimization of workpiece positioning for robot milling., Advances in Production Engineering & Management 12 (3) (2017), pp. 233–244.

[9] M. Halbauer, C. Lehmann, J. P. Städter, U. Berger, F. Leali, Milling strategies optimized for industrial robots to machine hard materials, in: Emerging Technologies & Factory Automation (ETFA), 2013 IEEE 18th Conference on, IEEE, 2013, pp. 1–4.

[10] S. Mousavi, V. Gagnol, B. Bouzgarrou, P. Ray, Model-based stability prediction of a machining robot, in: New advances in mechanisms, mechanical transmissions and robotics, Springer, 2017, pp. 379–387.

[11] Y. Altintas, Analytical prediction of three dimensional chatter stability in milling, JSME International Journal Series C Mechanical Systems, Machine Elements and Manufacturing 44 (3) (2001), pp. 717–723.

[12] G. Xiong, Y. Ding, L. Zhu, A feed-direction stiffness based trajectory optimization method for a milling robot, in: International Conference on Intelligent Robotics and Applications, Springer, 2017, pp. 184–195.

[13] J. Knapczyk, M. Ryska, Stiffness matrix analysis of six-revolute serial manipulator, acta mechanica et automatica 6 (2012), pp. 62–65.

[14] R. Featherstone, A divide-and-conquer articulated-body algorithm for parallel o (log (n)) calculation of rigid-body dynamics. part 1: Basic algorithm, The International Journal of Robotics Research 18 (9) (1999), pp. 867–875.

[15] M. L. Felis, Rbdl: an efficient rigid-body dynamics library using recursive algorithms, Autonomous Robots 41 (2) (2017), pp. 495–511.

[16] K. Museth, Vdb: High-resolution sparse volumes with dynamic topology, ACM Transactions on Graphics (TOG) 32 (3) (2013), pp. 27.

[17] S. Engin, Y. Altintas, Mechanics and dynamics of general milling cutters.: Part I: helical end mills, International journal of machine tools and manufacture 41 (15) (2001), pp. 2195–2212.

[18] Y. Boz, H. Erdim, I. Lazoglu, Modeling cutting forces for 5-axis machining of sculptured surfaces, in: 2nd International Conference, Process Machine Interactions, Vol. 14, 2010.

[19] M. Weck, Werkzeugmaschinen 5: Messtechnische Untersuchung und Beurteilung, dynamische Stabilität, Springer-Verlag, 2006.